# DLR'S CONTRIBUTIONS TO THE AIAA HIGH LIFT PREDICTION WORKSHOP SERIES

R. Rudnik, S. Melber-Wilkending, K. C. Huber[1], S. Crippa[2]
DLR, German Aerospace Center, Institute of Aerodynamics and Flow Technology,
Braunschweig, Germany

**Abstract**

Since the AIAA High Lift Prediction Workshop has been launched in 2010, DLR has continuously contributed with experimental and numerical results to this workshop series. With the objective to improve RANS analysis capabilities for high lift configurations, the complexity of the considered configurations has successively been increased starting with a finite swept wing with a three element high lift system in Workshop I to the DLR F11 wing/body high lift configuration in Workshop II. Currently, a JAXA wing/body/nacelle/pylon configuration is considered for workshop III. The paper summarizes DLR's numerical and experimental contributions to all three workshops. Moreover, some lessons learned with respect to DLR's contributions are highlighted.

## 1. INTRODUCTION

Based on the successful collaborative model of the AIAA Drag Prediction Workshop (DPW) series [1], AIAA initiated the High Lift Prediction Workshop (HiLiftPW) in 2009 with the aim to extend the thematic frame to the aerodynamics of high lift systems on commercial aircraft configurations. Thus, the focus is on tube and wing configurations with swept, medium-to-high-aspect ratio wings with deployed high lift devices. A main objective is to assess the numerical prediction capabilities of current-generation flow solvers. This refers primarily to aspects of grid generation and grid topology, numerical algorithms, and turbulence modeling. In this context, an attempt has been made to derive and continuously assess practical modeling guidelines for CFD predictions of high-lift flow fields. A prerequisite for such type of investigations is the determination of key elements of high-lift flow physics that are critical for numerical simulations in order to pave the way for the development of more accurate high fidelity simulation methods and tools. In the medium to long run, the overall objective is to enhance the CFD prediction capability for practical high-lift aerodynamic design and optimization tasks.

The workshops are set-up as open unbiased forums to assess, cross compare, and discuss a large variety of partner contributions of the international high lift aerodynamics community. Each of the three workshops concentrates on specific test cases, which have been selected, prepared, and provided for public access by the organizing committee. At present, the committee of the AIAA high lift prediction workshop is composed of members of Boeing Commercial Aircraft, Textron Aviation, Gulfstream Aerospace, NASA Ames and Langley Research Centers, Pointwise, Inc, the University of Wyoming, and the DLR's Institute of Aerodynamics and Flow Technology. Boeing Commercial Aircraft is chairing the committee. DLR is involved in technical activities and as a committee member since the start of the high lift prediction workshop series.

Each workshop consists of a preparatory phase covering the selection of a specific test case, the preparation of the experimental data and the generation of a set of mandatory computational grids and related test computations. The experimental data, onflow conditions, and grids are made available when approved by the organizing committee to the general public with a sufficient lead time ahead of a workshop. The workshop itself is typically held in conjunction with an AIAA conference. All participants have the chance to present and discuss their respective results. Based on these open forum discussions, the contributing parties have the opportunity to revisit and extend their computations and publish them in specific special session at subsequent AIAA conferences or elsewhere. As for other AIAA workshop series, the general approach of the High Lift Prediction Workshop has been to progressively increase the geometrical and thus the aerodynamic complexity of the test cases under consideration.

Up to now, two workshops have been completed. The third one is in the final stage of the data preparation. Workshop I, [2], [3], held in 2010, was concerned with the NASA trapezoidal wing (TRAP wing), a swept and tapered three element high lift wing. For Workshop II in 2013, the DLR F11 wing/body configuration with a full span three-element high lift system was selected as the reference configuration [4]. The current Workshop III is scheduled to take place in 2017 [5]. A focus will be laid on the inclusion of wing-mounted podded nacelles to a wing/body configuration to end up with a configuration which is representative for typical industrial high lift design and layout investigations on commercial aircraft. For this purpose, the so-called JSM model of the Japanese research center JAXA has been selected. In addition, NASA's Common research model (CRM) is proposed as a second test case. A three element high lift system has been designed for the CRM wing/body configuration, so that it's ready to be investigated numerically in order to prepare envisaged wind tunnel tests, once the model has been manufactured.

The paper describes DLR's numerical and experimental contributions to the workshop I and II and provides a short outlook for the activities in workshop III.

[1] formerly DLR, now German Dutch Wind Tunnels, DNW
[2] formerly DLR, now Airbus Operations

## 2. HIGH LIFT PREDICTION WORKSHOP I

A simple 3D high lift wing geometry has been selected for the first High Lift Prediction Workshop. NASA's trapezoidal (Trap) wing is a large chord, semi-span, three element high lift wing configuration mounted on a body pod. The experimental set-up is described in Ref. [6] . The model is shown in FIG. 1 as tested in the 14 x 22 low speed wind tunnel of the Langley Research Center under atmospheric conditions.

FIG. 1. NASA Trap Wing in the 14 x 22 wind tunnel of NASA LaRC

The model has a semi span of 2.16 m and a quarter chord sweep of 30°. The aspect ratio of 4.56 is comparatively low, the taper ratio amounts to 0.4. The baseline setting of the high lift devices corresponds to a slat deflection of 30° and a flap deflection of 25°. The onflow Mach number is M = 0.2 and the chord Reynolds Number $Re_c = 4.3 \times 10^6$.

To structure the investigations, three test cases have been defined by the organizing committee. Case 1 is a grid refinement study on a simplified configuration without slat and flap brackets. The grid refinement is to be carried out for two angles of attack, $\alpha$ = 13° and 28°. Maximum lift is reached at $\alpha \sim 33°$. Case 2 is concerned with a reduced flap deflection of $\delta_f$ = 20°. Finally, case 3 features the inclusion of slat and flap brackets in direct comparison to Case 1.

The main objectives to be addressed by DLR's contribution in the context of HiLiftPW-I have been:

- Assessment of prism-dominant vs. hex-dominant near wall grid topologies of hybrid unstructured grids.
- A grid refinement study for a 3D high lift configuration.
- Assessment of the capabilities of the differential Reynolds-Stress turbulence model vs. widely used eddy-viscosity models in the TAU code.
- Investigation of the influence of the mounting system (brackets) of the high lift devices on a wind tunnel model.
- Investigation of an alternative device setting.
- Investigation of different start-up procedures for the convergence process of the TAU flow solver

Selected examples of these investigations will be presented hereafter. A more comprehensive summary of DLR's investigations is provided in Ref. [7]

### 2.1. DLR Grid Generation

At the time of the workshop the vast majority of high lift aircraft configurations has been dealt with at DLR using the CentaurSoft hybrid grid generation system, see [8] featuring hybrid prism-dominated near-wall areas. At the same time, the SOLAR grid generation software, developed by ARA, QinetiQ, BAE Systems, and Airbus [9], had matured to a level that allows to handle high lift configurations using hexa-dominated structured areas. Thus, Workshop I served as a forum to cross-check both approaches on an identical configuration. A general challenge for DLR's hybrid unstructured grid generation efforts in all the high lift prediction workshops has been the consideration of so-called gridding guidelines, edited by the organizing committee. The guidelines are strongly aligned to structured grid generation approaches, which pose in some aspects a considerable but valuable challenge to the widely automated hybrid unstructured grid generation systems. For both approaches, DLR provided mandatory grids to the workshop. In both cases, grid families have been provided to allow grid resolution studies for DLR and other partners, who decided to run their codes on DLR grids.

#### 2.1.1. SOLAR Grid System

As mentioned before, the SOLAR hybrid unstructured grids are hexa-dominant near the aerodynamic surfaces of the configuration, allowing high quality cells geometries. The grid family consists of three levels, coarse, medium, and fine, featuring 12.3, 37, 110.7 mil. grid points. The corresponding number of normal wall layers is 35, 51, and 74. The single grids have been generated by applying a scaling factor of $3^{(1/3)}$ to the volumetric sources. FIG. 2 shows the surface resolution. More details can be found in Ref. [7].

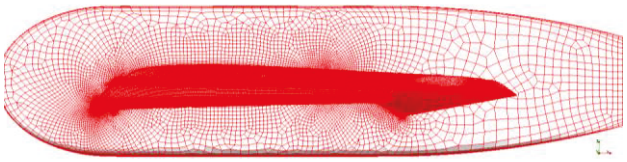

FIG. 2. Solar surface grid resolution on the medium level

#### 2.1.2. CENTAUR Grid System

In contrast to the SOLAR approach, the CENTAUR grids are characterized by prismatic near wall areas. Due to some difficulties in generating the fine grid while obeying the gridding guidelines, the CENTAUR grid family consists of three grid levels, designated as extra coarse, coarse, and a medium grid. The total number of grid points is 12.9, 16.4, 31.5 mil.. The corresponding no. of normal wall layers is 34, 36, and 38, respectively. The grid levels have been generated by employing a fully automatic source management developed by DLR.

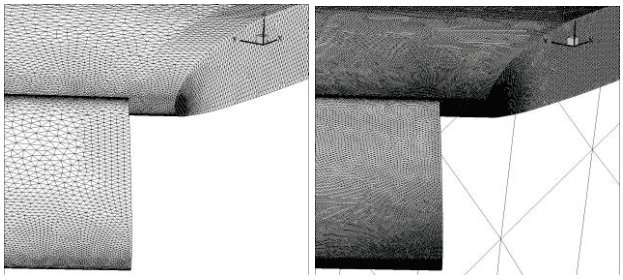

FIG. 3. CENTAUR surface grid resolution on the extra coarse (left) and medium (right) grid level

A close-up of the surface mesh for the extra-coarse and medium level at the tip of slat and fixed wing is shown in FIG. 3. For all meshes of both grid generation systems, a so-called y+ adaptation of the first wall spacing has been carried out according the respective Reynolds number.

## 2.2. DLR Numerical Results

DLR conducted TAU computations on both grid families. Major topics for these computations have been a grid resolution study, the assessment of the impact of turbulence modelling on the numerical results, as well as an investigation on the effects of the slat and flap brackets on the aerodynamic properties, see also [7].

### 2.2.1. Grid Resolution Study

The grid refinement, Case 1, concentrates on two angles of attack of the simplified configuration without slat and flap brackets. The flap brackets can be seen in FIG. 1. The Spalart-Allmaras turbulence model [10] has been used for all CFD computations concerning grid refinement. The angles of attack under consideration are $\alpha$ = 13°, representative for the linear lift range, and 28°, which is close to the configuration's maximum lift condition at $\alpha$ ~ 33°. FIG. 4 depicts the influence of the lift coefficient with the grid refinement achieved on the SOLAR and CENTAUR grid families for $\alpha$ = 28°. The grid point number N on the abscissa is scaled to the power of (-2/3). Using this scaling and the current numerical algorithm, a second order accuracy would be visible as a linear dependency of lift coefficient from the grid point number.

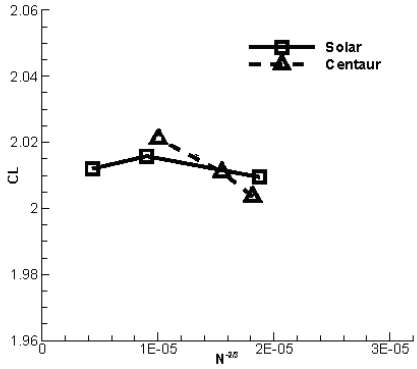


FIG. 4. Lift coefficients of the grid resolution study on the SOLAR grid family for $\alpha$ = 28°.

As expected, a certain deviation from the linear behavior can be seen. The variation of $\Delta C_L$ ~ 0.01 is fairly small taking the complex flow phenomena close to maximum lift conditions into account.

The analysis of the 9 spanwise pressure distributions reveals in general a small influence of the grid refinement. Moreover, a good agreement to the experimental pressure distributions is achieved, except for the most outboard station at 98% half span. Thus, this pressure distribution is the most relevance to analyze impacts of the numerical algorithm. FIG. 5 shows the computed pressure distributions on the SOLAR grids at this section together with the experimental evidence. The suction level at the fixed wing is in general underpredicted. This is even more pronounced for the flap pressure distribution. Increasing the grid density tends to improve this, but even on the finest grid a considerable deviation remains. The deviation appears not be overcome by further increasing globally grid resolution. Also for $\alpha$ = 13°, significant deviations between experiment and computation are found at the most outboard station, only. The magnitude of these deviations in the pressure distributions is smaller compared to those at the higher angle of attack.

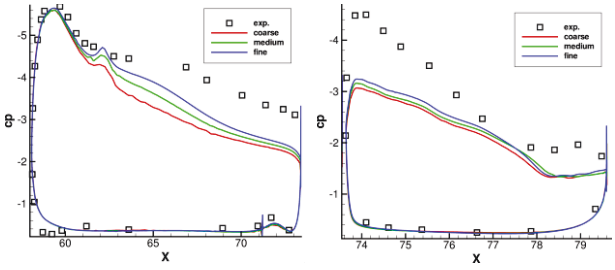


FIG. 5. Fixed wing and flap pressure distributions at $\eta$ = 0.98 for the SOLAR grid family for $\alpha$ = 28°.

FIG. 6 provides the same analysis for the CENTAUR grid family. The influence of the different grid resolutions is clearly smaller. Nevertheless, when comparing the results of both grid families it has to be kept in mind, that the range of grid points is much smaller for the variation using the CENTAUR grids. Moreover, the set-up of the grid refinement is less consistent compared to the one used for the SOLAR grid family.

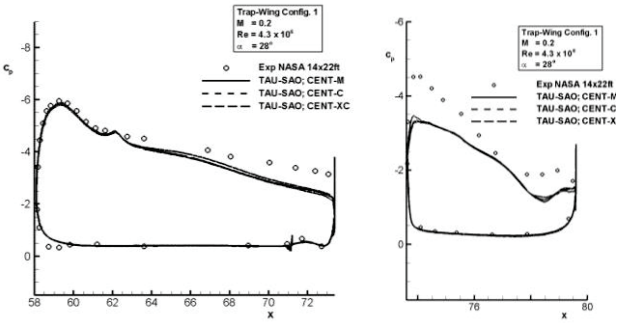


FIG. 6. Fixed wing and flap pressure distributions at $\eta$ = 0.98 for the CENTAUR grid family for $\alpha$ = 28°.

In order to identify the reason for the miss-prediction close to the wingtip, a flowfield analysis has been carried out. FIG. 7 gives an impression of the complex interactions at the wingtip for the smaller angle of attack. According to this simulation, the slat and fixed wing edge vortices interact with the boundary layer above the rear main wing and the flap. The structure of the main element and slat

side edge vortices above the outboard flap suggests a vortex breakdown. As a consequence, the induced velocities of the vortices on the aerodynamic surfaces will be reduced. If such a vortex breakdown occurs premature in the numerical simulations, it can cause the observed underprediction of the suction levels on the upper surfaces of main wing and flap at the outboard pressure section.

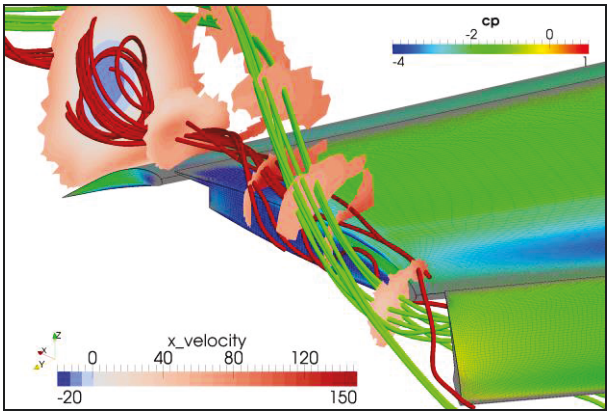


FIG. 7. Isobars and streamlines at the wing tip computed on the SOLAR grid for $\alpha$ = 13°.

Due to the lack of experimental flowfield evidence, this assumption could not be validated so far.

### 2.2.2. Comparison of TAU Results on SOLAR and CENTAUR Grids

For the direct comparison of TAU results using SOLAR and CENTAUR grids, results with the Spalart-Allmaras turbulence model (SAO) have been evaluated on the medium level grids. In general, deviations between the results on the two grids are very small. Again the differences become obvious on the most ouboard pressure section, shown in FIG. 8.

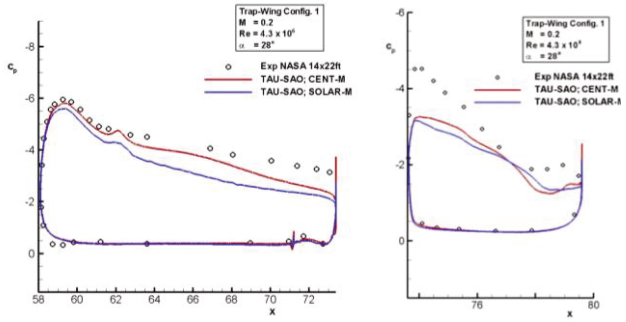


FIG. 8. Fixed wing and flap pressure distributions at $\eta$ = 0.98 for the SOLAR and CENTAUR grid, $\alpha$ = 28°.

Using the SAO turbulence model, both solutions exhibit the afore mentioned deficits of not meeting the upper surface suction level. Yet, the solution on the CENTAUR grid shows smaller differences to the experimental pressure data.

### 2.2.3. Turbulence Model Influence

A variation of the turbulence model has been carried out on the medium CENTAUR grid. In addition to the Spalart-Allmaras model (SAO), the k - $\omega$ SST model (SST), according to Ref. [11], has been applied for this purpose, as well as the differential SSG/LRR-$\omega$ Reynolds-Stress model (RSM) developed by DLR [12]. The results are almost identical and in very good agreement to the experimental data for most of the configuration. As before, differences between the models are visible for the section at $\eta$ = 0.98, see FIG. 9.

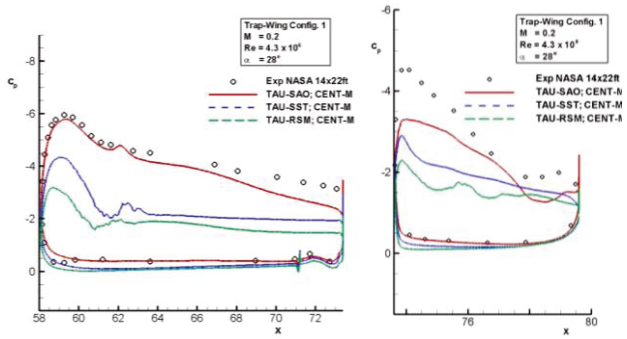


FIG. 9. Fixed wing and flap pressure distributions at $\eta$ = 0.98 for the SOLAR and CENTAUR grid, $\alpha$ = 28°.

Both, the SST as well as the RSM model tend to generate a strong separation on the fixed wing and the flap. The result produced with the SAO model exhibit the smallest, yet still significant deviations to the experimental data. It has to be noted, that this statement holds for the medium size CENTAUR grid and the configuration without the brackets assuming fully turbulent flow. Up to now, now special effort to improve the grids by locally resolving the vortex transport and interaction areas has been made. The corresponding lift curves are depicted in FIG. 10.

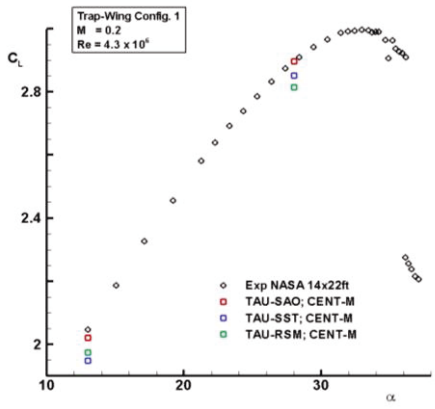


FIG. 10. Lift coefficients of the turbulence model variation on the CENTAUR grid family for $\alpha$ = 28°.

The trends as observed locally in the pressure distributions close to the wingtip in FIG. 9 are consistently reflected in the overall lift coefficients. The SAO model produces the highest lift coefficients closest to the experimental values for both considered angles of attack.

## 3. HIGH LIFT PREDICTION WORKSHOP II

In order to successively increase the complexity of the considered configurations, a wing/body high lift configuration appears to be the next logical step in complexity. As a baseline for the second High Lift

Prediction Workshop, the DLR-F11 high lift configuration has been selected. This high lift configuration has been set-up and wind-tunnel tested in the framework of the European research projects EUROLIFT, and EUROLIFT II [13]. For HiLiftPW-II, the full span slat and flap wing/body configuration is considered with gapless slat and flap junctions at the fuselage, see FIG. 11.

FIG. 11. DLR-F11 high lift configuration mounted in the low speed wind tunnel B-LSWT

The release of the dataset has been requested by DLR and granted by the EUROLIFT consortium and by the EC. Due to the challenge to adequately resolve all flow features and carry out grid convergence studies, also this configuration is considered in an 'as-tested' as well as in a simplified version. The geometric simplification concerns the slat tracks, the flap track fairings, and pressure tube bundles that are externally attached to the slat tracks, see FIG. 12

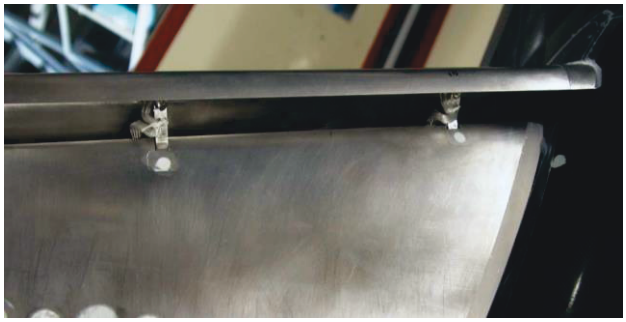

FIG. 12. Slat tracks and pressure tube bundles on the DLR-F11 high lift configuration, view from below.

The model is representative for a modern commercial aircraft configuration. It has a half span of 1.4 m and a quarter chord sweep of 30°. The aspect ratio of 9.35, the taper ratio amounts to 0.3. The baseline setting of the high lift devices corresponds to a slat deflection of 26.5° and a flap deflection of 30°. A major new aspect of the investigation on the F11 configuration is the option to compare low and high Reynolds number test data. The model has been tested in identical configurations in the low speed wind tunnel of Airbus in Bremen, B-LSTW, at a chord Reynolds Number $Re_c$ = 1.35 x $10^6$ and at ETW in Cologne at $Re_c$ = 15 x $10^6$. The Mach number in both tests has been M = 0.175. Details of the configuration and the experimental dataset are provided in [14].

For the second workshop, four test cases have been defined by the organizing committee. Case 1 picks up the grid convergence study, now to be applied to the more complex configuration. Case 2 adds a Reynolds Number study as a new aerodynamic aspect. Case 3 is concerned with the investigation of details of the wind tunnel model. For the DLR-F11 configuration, this covers the inclusion of flap tracks fairings, slat racks, and the pressure tube bundles in separate complexity stages. Finally, Case 4 is a turbulence model verification study on simple test cases, intended to ensure that all participants have consistent implementations of the various turbulence models.

The main objectives to be addressed by DLR's contribution for HiLiftPW-II have been:

- Refurbish and provide a unique experimental data set containing in-depth experimental evidence such as Particle Image Velocimetry data, boundary layer probe measurements, hotfilm and infrared transition information. The data have been measured in the frame of the EUROLIFT project. The intention has been to compile and preserve the dataset and provide public access to allow further explorations.

- Extension of the grid refinement study for a representative 3D high lift wing/body configuration based on SOLAR grid generation system.

- Simulation of Re-No. scaling effects on $C_{L,max}$. including Re-adapted gridding capabilities.

- Capability to assess "secondary" configuration details and configuration simplifications.

As for the first workshop, selected examples of these investigations will be presented.

### 3.1. Experimental Dataset for the DLR F11 High Lift Configuration

The DLR F11 high lift configuration has been investigated experimentally and numerically in the European projects EUROLIFT and EUROLIFT II [13]. The first project lasted from in 2000 to 2003 and was dealing with the wing/body configuration, making it a suitable candidate for the use in the High Lift Prediction workshop. A comprehensive dataset has been collected and could only be partly explored within EUROLIFT. Releasing the dataset for the use in the High Lift Prediction Workshop allowed a more detailed evaluation of the experimental data, the compilation of the data, their preservation, and use for a large scale validation exercise. Two tests have been carried out on the wing/body configuration. The first one took place under atmospheric and thus sub-scale conditions in the low speed wind tunnel B-LSWT of Airbus in Bremen. It provided a comprehensive dataset consisting of forces and moments, high resolution steady surface pressure measurements, PIV measurements, hotfilm and infrared thermography for transition detection, as well as oil flow measurements for flow visualization.

As an example, FIG. 13 shows an oil flow visualization recorded in the B-LSWT for low Reynolds number conditions for increasing angles of attack. The traces of the slat tracks and the pressure tube bundles are clearly visible on the fixed wing upper surface. Especially midboards, the traces widen up strongly and obviously strongly influence the lift breakdown at the higher angles of attack. The oil flow pictures underline the necessity to consider supposedly secondary geometrical influence in order to consistently compare numerical and experimental results.

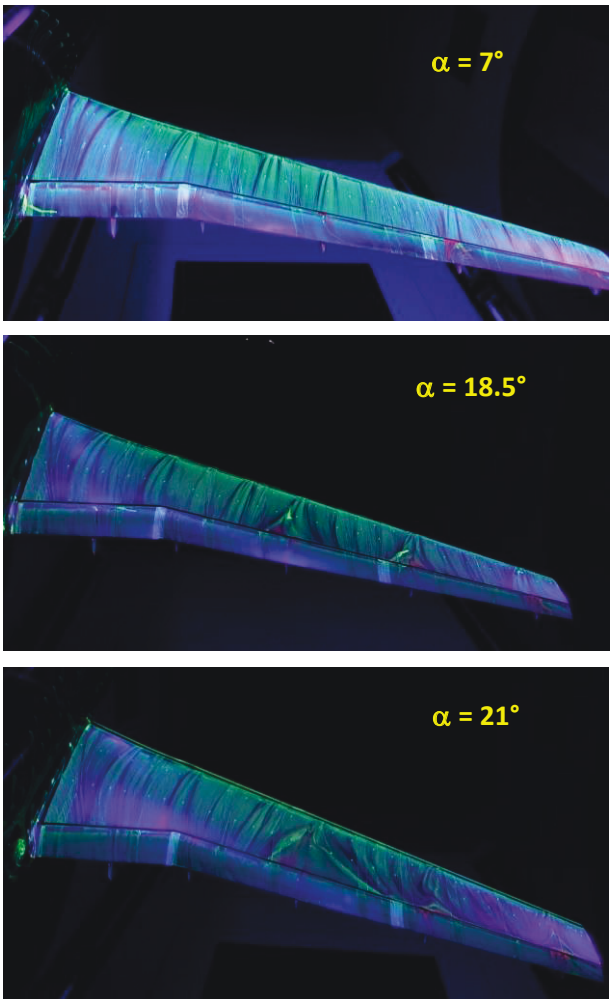


FIG. 13. Oil flow pictures for different angles of attack under low re-conditions in the B-LSTW

An example of the PIV measurements is provided in FIG. 14.

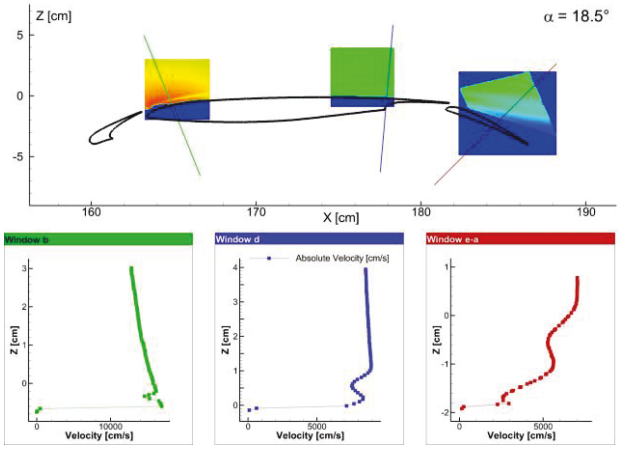


FIG. 14. PIV measurement windows and extracted velocity profiles taken in the B-LSTW

The three observation windows have been placed above the fixed wing downstream of the slat, in the vicinity of the fixed wing trailing edge, and above the flap in three wing sections. The lower part of the window depicts velocity profiles above the fixed wing and flap surface. To derive these profiles, the instantaneous camera pictures had to be time-averaged. Then, the velocities along the target lines have to be interpolated based on the vector field information of the measurements. Flowfield information has proven to be very valuable in further analyzing the quality of the CFD results and deriving relivable assessments of turbulence modeling or grid resolution influences.

The high Reynolds number tests have been carried out under cryogenic high pressure conditions in the ETW. Due to the challenge to carry out measurements under these conditions, the available data for high Reynolds numbers are restricted to classical force and moment measurements as well as pressure distributions along all elements of the wing.

### 3.2. TAU Code Results for the DLR F11 High Lift Configuration

Major aspects of DLR's numerical investigations for the second workshop have been devoted to the assessment of the capability to predict the effects of Reynolds scaling on the high lift performance and to investigate the influence of model simplifications.

#### 3.2.1. Grid Generation for the DLR F11 Configuration

The grid generation effort for the HiLiftPW-II was carried out using the SOLAR grid generation package. The focus was laid on the stepwise consideration of configuration details designated as configuration complexity stages. As a baseline, flap and slat are investigated in a reference setting for the landing configuration. This configuration consisting of wing/body including a functional surface at the wing/fuselage intersection is denoted as complexity Stage II. The second considered configuration is derived from Stage II by the inclusion of 5 flap track fairings and 7 slat tracks, leading to configuration Stage IV. The most complex configuration, Stage V, includes additionally pressure tube bundles, which have been externally mounted to the slat tracks due to lack of internal installation space in the slat itself or the tracks.

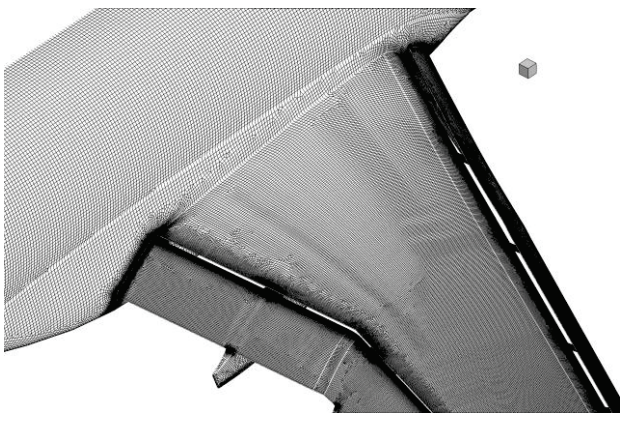

FIG. 15. SOLAR surface grid for the DLR-F11 high lift configuration, Stage V, on the medium grid level

Hybrid hexa-dominant grids have been generated on a medium level for all three complexity stages. Moreover, the grids have been adapted to both considered Reynolds

numbers to provide adequate boundary layer resolution. The medium grid levels for the various complexity stages feature overall grid point numbers between 26 and 38 mil.. FIG. 15 show the inboard part of the surface mesh for the most complex configuration stage V. In addition to the various medium grids, a grid family with coarse, medium, and fine grid have been generated for complexity Stage II, ranging from 9 to 74 mil. grid points.

### 3.2.2. Simulation of Re-No. Scaling Effects on the High Lift Performance

According to the experimental evidence, the Reynolds number has been varied by more than one order of magnitude from $Re_c = 1.35 \times 10^6$ in the B-LSWT up to $Re_c = 15 \times 10^6$ in the ETW. The ETW Reynolds number is in the range of real aircraft conditions. Studies in EUROLIFT proved that for this configuration favorite Reynolds number effects are found. Both, the lift coefficient and especially $C_{L,max}$ are increasing with Reynolds number. FIG. 16 shows midboard pressure distribution on the elements of the high lift wing for a medium to high angle of attack of $\alpha$ = 16° for low and high Reynolds number conditions.

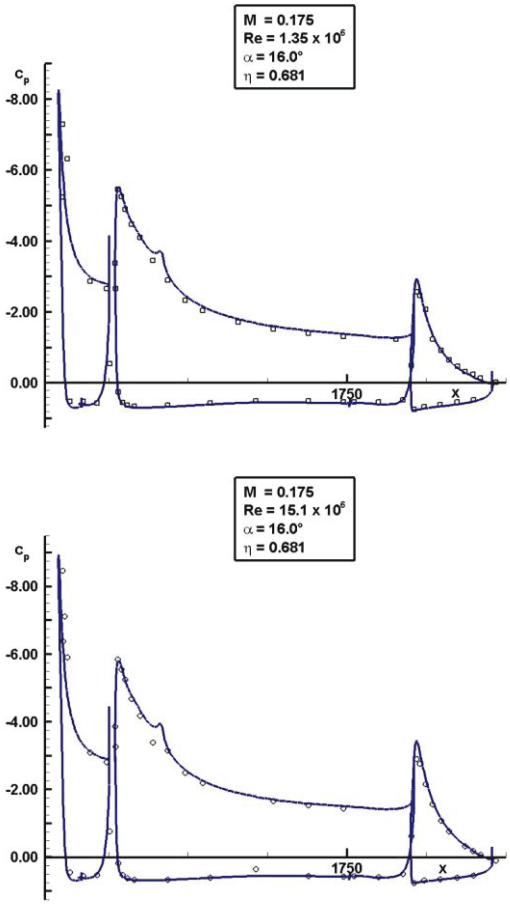


FIG. 16. Midboard pressure distribution on all high lift elements for low (top) and high (bottom) Reynolds number conditions at $\alpha$ = 16°.

Comparing the low Reynolds number results in the upper half of the Figure to the high Reynolds number results in the lower part reveals that the suction peaks as well as the general suction levels are as expected higher for the high Reynolds number conditions. This is consistent with first order Reynolds number effects, which tend to reduce the friction effects and the related de-cambering of a flow along a wing due to the smaller boundary layer heights. Consequently, a higher lift is obtained at the high Reynolds number test. In general, a good agreement is observed between the TAU computations, see blue lines, and the experimental evidence (black symbols). The computations have been carried out using the Spalart-Allmaras turbulence model and the medium grid refinement level. FIG. 17 shows the resulting computed and measured lift curves for both Reynolds numbers with the same color coding.

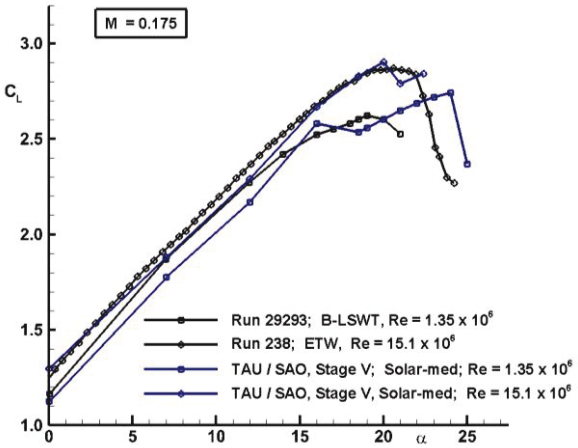


FIG. 17. Computed and measured lift curves for midboard for low and high Reynolds number conditions.

The experimental data indicate an increase in lift coefficient of about 0.15 in the linear lift regime and a maximum lift coefficient, which is 0.25 higher for the increased Reynolds number. $\alpha_{max}$ is increased by nearly two degrees. The slope of the experimental lift curve shows a more pronounced linear lift regime for the higher Reynolds number up to about $\alpha$ = 15°. Maximum lift is exceeded in a well-rounded way indicating the same smooth lift breakdown for both Reynolds number conditions. The computed lift curves reveal a better agreement to the ETW data in the linear lift range. $C_{L,max}$ is overpredicted by 1.5%, at the same time, $\alpha_{max}$ is underpredicted by about 1°. The lift increase and the extended linear lift regime due to the high Reynolds number conditions are well captured by CFD. Nevertheless, the distinct rounded slope of the lift curve at low Reynolds number conditions between 5° and 15° causing the reduced lift increment between low and light Reynolds number conditions, is not reflected by the computations.

### 3.2.3. Assessment of Model Details and Configuration Simplifications

The numerical approach via CFD allows to separate influences of geometrical features of a wind tunnel model. This aspect has been intensively studied on the DLR-F11 high lift configuration with several so called complexity stages as described above. A corresponding study has been carried out by DLR for high Reynolds number

conditions on the medium grid level. FIG. 18 shows the resulting lift curves for the considered complexity Stages II, IV, and V.

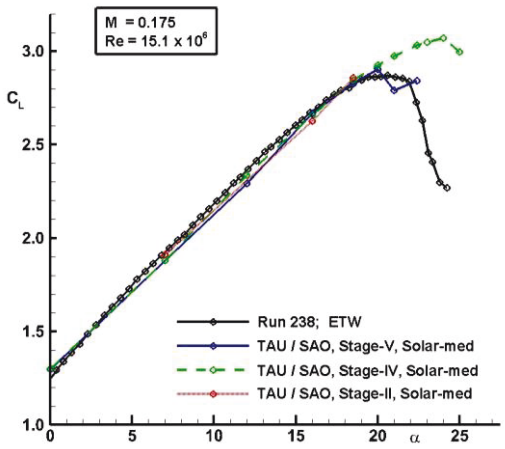


FIG. 18. Slat tracks and pressure tube bundles on the DLR-F11 high lift configuration, view from below.

Analyzing the three lift curves shows that the impact of these geometric details is comparatively small in the linear lift range. Comparable computations are available for $\alpha$ = 7°, $\alpha$ = 16°, and $\alpha$ = 18.5°. Interestingly, the lift coefficient $\alpha$ = 16° for the most simplified and "clean" configuration, Stage II, is lower than the one of the other two configurations. The expectation is that these aerodynamic disturbances and their impact cause a lift reduction. This is the case for the smaller and larger considered angles of attack, $\alpha$ = 7° and 18.5°, although the lift reduction is quite moderate. Comparing stages IV and V around maximum lift reveals that the pressure tube bundles do have a significant effect here. The primary lift breakdown in the blue curve at $\alpha$ = 21° is obviously caused by the influence of the tube bundles. It has been observed for configurations Stage V for low and for high Reynolds numbers.

A more detailed and comprehensive description of DLR's numerical activities in Workshop II is given in [16], the influence of the Reynolds number scaling effects is discussed in [17].

## 4. HIGH LIFT PREDICTION WORKSHOP III

High Lift Prediction Workshop III is in the preparation phase. The relevant CAD geometry data, mandatory grids, and the experimental evidence are about to be published. The configurative basis for the third workshop is twofold. Following the concept of a stepwise increase in complexity, pylon and nacelle are added to the wing/body configuration to be able to consider aerodynamic interference effects of the propulsion/airframe integration. This study is designated as Case 2. For this purpose, the so-called JAXA Standard Model (JSM) has been selected as a reference configuration. It is a commercial aircraft type half model in high lift configuration, tested in the 6.5m x 6.5m low speed wind tunnel at the JAXA research center. The model has a half span of 2.3 m and a leading edge sweep of 33°. The aspect ratio is $\Lambda$ = 9.42, the taper ratio amounts to 0.3. The baseline setting of the high lift devices is given by a slat deflection of 25° and a flap deflection of 30°. The model has been tested in the low speed wind tunnel at a chord Reynolds Number $Re_c$ = 1.93 x $10^6$. The test Mach number is M = 0.172. Details of the configuration and the experimental dataset are provided in Ref. [18]. The JSM model in the JAXA wind tunnel is depicted in FIG. 19.

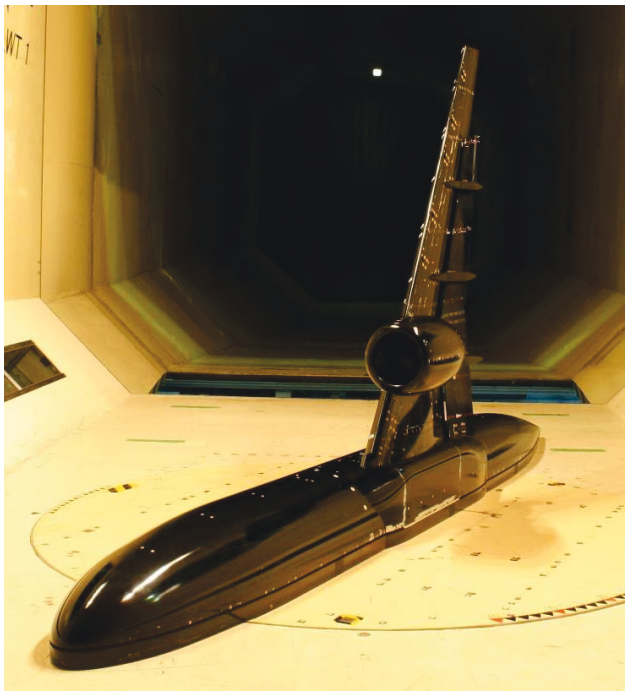

FIG. 19. JAXA JSM high lift configuration

Again, a large body of aerodynamic test data is released for this test case. Among these are force and moment data, surface pressure distributions and oil flow pictures. An example for the latter is provided in FIG. 20.

FIG. 20. Oil flow visualization for the JAXA JSM high lift configuration

The complex interaction between the nacelle and pylon and the airframe is clearly visible in the oil flow picture. A special challenge for the grid generation is posed by the fact that the deployed slat is partly intersecting with the fixed wing.

Due to the availability of a high lift system for the NASA Common Research model [19], an alternative configuration is considered with the CRM wing/body high

lift model. Given the lower complexity of the wing/body high lift configuration, Case 1 addresses a grid convergence study on the CRM. No experimental data will be available for this configuration at the third workshop. Thus, Case 1 is intended to be a pure CFD verification study.

Up to now, DLR has generated grids for the JSM wing/body configuration and the one with installed nacelle and pylon. Again, the SOLAR grid generation software is used to set-up the computations grids. The grid for the installed configuration features 128 mil. grid points. A view of the surface grid is provided in FIG. 21.

FIG. 21. SOLAR surface grid for the JAXA JSM high lift configuration on the medium grid level

A close-up of the grid at wing/pylon intersection is provided in FIG. 22., underlining the near wall structured grid topology.

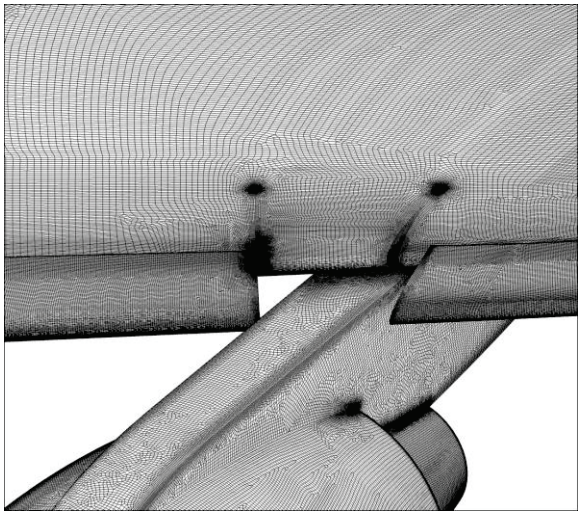

FIG. 22. Detail of the SOLAR surface grid for the JAXA JSM configuration at the wing/pylon intersection

TAU computations of the lift curves for the JSM high lift configuration are at present carried out using the RSM turbulence model. The results will be presented at the third High Lift Prediction Workshop in 2017.

## 5. CONCLUSION

The paper describes activities of DLR's institute of Aerodynamics and Flow Technology in the framework of the AIAA High Lift Prediction Workshop series. The overall objective of the workshops is to test, analyze, and assess numerical prediction capabilities to characterize the aerodynamics of high lift commercial aircraft configurations. DLR has contributed to the workshops since 2009 by both, numerical and experimental data. For the numerical part, DLR's flow solver TAU has been used together with computational grids that have been generated and provided by DLR using the CentaurSoft and SOLAR grid generation software. DLR contributed to the common computations by providing committee grids and numerous flow solutions as well as by providing the experimental database for the second workshop.

The first workshop dealt with a simple three element high lift wing. Except at the wingtip, a good agreement to the experimental evidence is achieved in terms of pressure distributions and global coefficients. DLR's investigation proved that the overall influence of the spatial resolution is quite small for globally refined grid families. The hex-dominated and the prism-dominated near wall grid topologies provided similar results. The resolution on the medium grid appears appropriate for the considered configuration, except at the wing tip, where vortex dominated aerodynamic phenomena could not be adequately captured. The application of more sophisticated turbulence models up to a differential Reynolds stress model could not improve the predictions on the medium resolution grids. Local grid refinement or adaptation holds promise to improve the simulations, but has not been yet investigated in detail.

For the second workshop, a more realistic configuration has been selected with the DLR F11 wing/body model with a three element high lift system. Reynolds number scaling effects have been investigated together with model simplification using TAU and the Spalart-Allmaras turbulence model. In general, a good agreement between CFD computations and experimental evidence is observed. Effects of configurative simplifications on the high lift aerodynamics could be emphasized by the numerical approach. Yet, deviations between the simulated effects of slat tracks and pressure tube bundles with respect to separation tendencies and lift breakdown remain.

In general, the contributions to both workshops provided substantial guidance for the numerical simulation of commercial aircraft high lift configurations at DLR. This concerns strategies for the most suited grid generation approach, turbulence modelling, numerical features, and physical effects for high lift flows. Yet, the deviations between CFD and experimental evidence indicate that still substantial improvements have to be made to meet the industrial accuracy requirements for high lift performance prediction. The AIAA High Lift Prediction Workshops are regarded as a valuable forum to benchmark own capabilities against the international state-of-the-art in high lift aerodynamics and guide future developments in high lift simulation.

Therefore, DLR will continue its participation with the third AIAA High-Lift Prediction Workshop scheduled to take

place in 2017. Numerical activities concerning grid generation and CFD computations are at present ongoing.

## 6. REFERENCES


[1] K. R. Laflin, “AIAA CFD Drag Prediction Workshop: An Overview”, 25th Congress of International Council of the Aeronautical Sciences, 3 - 8 September 2006, Hamburg, Germany, Paper ICAS 2006-2.4.1 (2006)

[2] Slotnick, J. P., Hannon, J. A., and Chaffin, M., “Overview of the First AIAA CFD High Lift Prediction Workshop” AIAA Paper 2011-862 (2011).

[3] Rumsey, C. L., Slotnick, J. P., Long, M., Stuever, R. A., and Wayman, T. R., “Summary of the First AIAA CFD High-Lift Prediction Workshop,” Journal of Aircraft, Vol. 48, No. 6, 2011, pp. 2068–2079.

[4] Rumsey, C. L., Slotnick, J. P, “Overview and Summary of the Second AIAA CFD High Lift Prediction Workshop” AIAA Paper 2014-0747, ,(2014).

[5] / 3rd AIAA CFD High Lift Prediction Workshop (HiLiftPW-3), www.hiliftpw.larc.nasa.gov

[6] Johnson, P. L., Jones, K. M., and Madson, M. D., “Experimental investigation of a simplified 3D high lift configuration in support of CFD validation", AIAA Paper 2000-4217 (2000).

[7] Crippa, S., Melber-Wilkending, Rudnik, R. “DLR Contribution to the First High Lift Prediction Workshop”, AIAA Paper 2011-0938 (2011).

[8] Kallinderis, Y., “Hybrid Grids and Their Applications", Handbook of Grid Generation, edited by J. F. Thompson, B. K., Soni, and N. P. Weatherill, chap. 25, CRC Press, 1999.

[9] Leatham, M., Stokes, S., Shaw, J. A., Cooper, J., Appa, J., and Blaylock, T., “Automatic Mesh Generation for Rapid-Response Navier-Stokes Calculations" FLUIDS 2000 Conference and Exhibit, June 2000, AIAA 2000-2247.

[10] Spalart, P. R. and Allmaras, S. R., “A One-Equation Turbulence Model for Aerodynamic Flows", La Recherche Aerospatiale, Vol. 1, 1994, pp. 5-21.

[11] Menter, F. R., “Two-Equation Eddy-Viscosity Turbulence Models for Engineering Applications" AIAA Journal, Vol. 32, 1994, pp. 269-289.

[12] Eisfeld, B., “Numerical Simulation of Aerodynamic Problems with the SSG/LRR-ω Reynolds Stress Turbulence Model Using the Unstructured TAU Code" New Results in Numerical and Experimental Fluid Mechanics VI , Vol. 96 of Notes on Numerical Fluid Mechanics and Multidisciplinary Design, Springer-Verlag, 2007, pp. 356-363, 15. DGLR/STAB-Symposium (2007).

[13] R. Rudnik, P. Thiede, “European Research on High Lift Aircraft Configurations in the EUROLIFT Projects”, CEAS/KATnet Conference on Key Aerodynamic Technologies, CP, 2005, pp. 16.1-16.8.2005 (2005)

[14] R. Rudnik, K. Huber, S. Melber-Wilkending, „EUROLIFT Test Case Description for the 2nd High Lift Prediction Workshop”, AIAA paper 2012-2924 (2012).

[15] R. Rudnik, “Experimental Analysis of Separation and Transition Phenomena for the DLR-F11 High Lift Configuration, AIAA Paper 2013-3035 (2013).

[16] R. Rudnik, S. Melber-Wilkending, “DLR Contribution to the 2nd High Lift Prediction Workshop”, AIAA 2014-0915 (2014).

[17] R. Rudnik, Germain, E., “Reynolds-Number Scaling Effects on the EUROPEAN High Lift Configurations”, Journal of Aircraft, Vol. 46, No. 4, July-August 2009, pp. 1140-1151. (2009)

[18] Ito, T., Yokokawa, Y., Ura, H., Kato, H., Mitsuo, K., and Yamamoto, K., “High-Lift Device Testing in JAXA 6.5M X 5.5M Low-Speed Wind Tunnel,” AIAA Paper 2006-3643, 2006.

[19] D. S. Lacy, A. J. Sclafani. "Development of the High Lift Common Research Model (HL-CRM): A Representative High Lift Configuration for Transonic Transports", AIAA paper 2016-0308 (2016)